# *An Investigation into the Mechanism of Dust Generation in a Tumbling Mill*


***Sam W. Kingman****
***Ian S. Lowndes****
***Evagellia Petavratzi*****
***David N. Whittles******

** School of Chemical and Environmental Engineering, University of Nottingham, Nottingham, NG7 2RD, UK*
*Email: ian.lowndes@nottingham.ac.uk*

*** Scott Wilson Ltd, Chetwynd Business Park. Chilwell. Nottingham. NG9 6RZ, UK*

**** Arup Ltd, The Arup Campus, Blythe Gate, Blythe Valley Park, Solihull, Birmingham, West Midlands, B90 8AE, UK*

## ABSTRACT

The generation of dust from mineral extraction and processing sites is related to the mechanisms of formation exhibited by the various minerals handling processes which are undertaken. For example processes such as sieving, grinding, transfer of materials with conveyor belts might generate dust fractions by abrasion, and the use of draglines or the tipping of material are liable to generate dust due to impaction. Previous research investigations have attempted to quantify dust levels by the development of a variety of laboratory based dustiness tests, which simulate common handling processes. These laboratory tests can be very useful tools for quantitative studies of the dust generation potential of materials if they relate accurately to the process under investigation. This paper presents the development of an experimentally validated model to improve the fundamental understanding of the breakage mechanisms associated with the dust generated by of one of the most popular dustiness tests, the HSE-WSL rotating drum apparatus applied to rock samples obtained from a large UK limestone quarry. This investigation employed both an experimental and computational approach. The experiments conducted explored the kinetics of the tumbling action for a variety of single sized limestone fractions. The resultant breakage processes produced by the mill were modelled using the specific rate of breakage and the breakage distribution function determined from experiment. Further experimental investigations were performed using a high speed video system to identify both the dynamics of the limestone charge in the tumbling mill, and the participating breakage mechanisms. Finally, a computational discrete element model (DEM) was employed to predict particle motion, fragmentation and energy distribution in the tumbling mill. A comparison of the experimental and computational results have concluded that the generation of the resultant dust fraction is

solely due to abrasion caused by the frictional sliding of particles on the drum walls and over other particles. This conclusion indicates that the HSE-WSL mill replicates the industrial processes that they are liable to produce particulates by abrasion (e.g. conveyor belts, sieving, mills). The breakage process of the tumbling mill followed the first order kinetics hence the tumbling action can be predictable. The subsequent DEM models have verified that operational parameters of a process such as the rotational speed, the power draw and the sample mass are closely relevant to the dust generation potential of a material. This in depth investigation of the involved mechanisms in industrial processes has proved to compare well with the liberation dust and it may be used to predict trends and evaluate the impact of a specific event.

***Keywords*:** DEM modelling; Dust generation potential; WSL tumbling mill; Particle motion; Experimental dustiness test

## 1. INTRODUCTION

The dustiness of a material is defined as being a measure of its propensity to generate dust from a bulk source (Higman, 1985). Dustiness is closely dependent on the materials handling processes which are taking place (e.g. materials transport and comminution). An understanding of and the ability to predict the dustiness of a material is important as dust is potentially hazardous to the environment, the human health, the safety and the productivity of a processing plant. In addition, air quality standards and occupational health limits, aim to delimit, prevent and control particulate matter emissions originated by the industrial sector (Petavratzi et al., 2005).

To try and quantify the dust generation potential during certain material handling processes a range of dust measurement techniques have been developed. These dustiness tests can be categorised into the following three groups (British Occupational Hygiene Society Technology Committee, 1985; Higman, 1985; Lyons and Mark, 1994; Schneider and Hjemsted, 1996):

(i) Impact or single drop methods. The test material falls from a certain height onto a metal surface in an enclosed chamber.
(ii) Fluidization methods. A current of air passes through a bed of coarse particles mixed with the test material at a sufficient velocity to overcome the inter-particle bed forces and to cause dispersion.
(iii) Rotating drum methods. The test material is repeatedly lifted by a series of blades and dropped into the drum chamber as it rotates.

The use of rotating drum tests has been most popular as they are the most versatile. They have the advantage that fine, lumpy, dry or damp material can be easily tested, allowing a range of mass concentrations and size fractions (powders, pellets, granular material) to be selected. The dust measurement tests provide a quantitative measure of the particulate matter generation potential of different materials. This paper reports the results of an experimental and computational investigation to identify the dust generation mechanisms present within a WSL dustiness test drum (HSE-WSL).

In the mining industry dust can potentially be generated and emitted during all stages of extraction, preparation and processing. In a recent research investigation (Petavratzi et al., 2007) a series of rotating drum dustiness tests were undertaken on a crushed pure limestone from a Derbyshire quarry in the UK using the Warren Spring Laboratory (WSL) rotating drum test method (HSE-WSL). The findings of this work revealed that the mass and size distribution of the sample charge, tumbling time and the amount of initial fines all influenced the final dust yield. These findings are significant because they indicate that the volume of dust produced depends upon both the operational parameters and material properties. An understanding of these relationships may therefore assist the estimation of possible dust sources associated with the various stages of a mineral flow sheet.

Although dustiness tests provide a method of quantifying the propensity of material to produce dust, the dustiness prediction is valid only for those processes for which the mechanism of dust production is replicated by the test method. The test method, therefore, has to simulate the relevant mechanism of dust production for the result to be meaningful. The objective of the research presented in this paper was to investigate the mechanism responsible for dust production that occurs in the HSE-WSL rotating drum test and hence identify the actual processes which these mechanisms simulate. For these experimental and theoretical investigations a crushed-high-purity-limestone particles obtained from a local Derbyshire quarry in the UK were used.

The mechanisms of dust generation in the tumbling mill were investigated using both experimental and computational methods. Experimentation took place through two different procedures. Initially the kinetics of the tumbling action were explored for a variety of single sized limestone fractions, by conducting the WSL test for a range of tumbling times and surveying the effect which the rotation period has on the test samples. The specific rate of breakage of each mineral fraction tested was calculated and conclusions were drawn upon the probability of the limestone fractions to break and generate dust. The behaviour of the limestone particles in the drum during the rotating action was further investigated and recorded using a high speed video system. The high speed camera assisted the understanding of the dynamics of the limestone charge in the tumbling mill, and the participating breakage mechanisms identified. In addition, the tumbling mill was simulated through computational steps using the discrete element modelling (DEM) method. The DEM model was constructed to provide a more fundamental understanding of the particle motions, the fragmentation processes and the energy distributions within the tumbling mill. The results of the experimental and computational studies were compared and conclusions drawn regarding the mechanisms causing dust generation and the effectiveness of the WSL rotating drum test to simulate common processes of mineral sites with high dust production potential.

## 2. BREAKAGE MECHANISMS IN COMMON GRINDING MILLS AND THEIR RELATION TO DUST GENERATION

Although the HSE-WSL tumbling mill is not a grinding mill, nevertheless some of the mechanisms of dust production associated with tumbling mills will occur in grinding mills as the operational principles are similar. In grinding mills, such as autogenous

mills, there are various mechanisms that take place, which result in particles breakage and diminishing particle size. During tumbling, particles are lifted to the top of the mill and subsequently move perpendicular to the plane of contact, impacting on other particles or on the drum walls, which produce breakages (Fig. 1). At the same time, part of the charge is active in producing abrasion and attrition breakage due to inter-particle contacts and particle-wall contacts (Napier-Munn et al., 1996). Mineral processing engineers often investigate the breakage patterns found in grinding mills so as to optimise their performance (e.g. minimise energy consumption, and fines concentration) and to increase throughout.

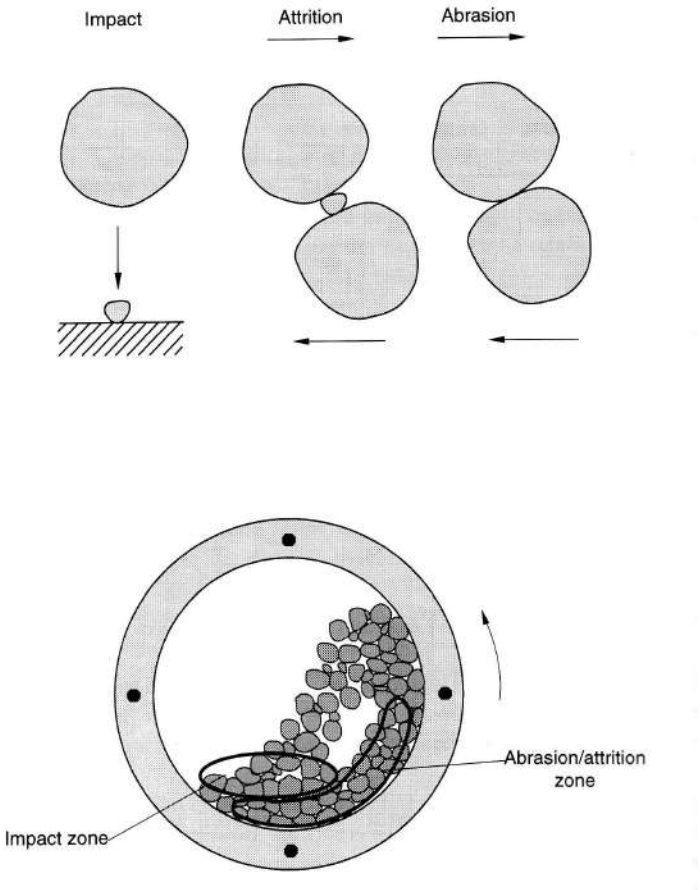


Fig. 1- The tumbling action and associated breakage mechanisms (Napier-Munn, Morrell, Morrison, and Kojovic 1996)

A similar investigative approach may be taken to investigate the breakage events within a HSE-WSL dustiness tumbling drum, to determine if the breakage of the test particles is responsible for the generation of dust and to identify what are the principle mechanisms acting on the particles of this particular test that contribute to the production of fine particulate matter. In addition, more fundamental understanding of the dust generation process of the tumbling test can allow critical comparisons to be made upon the industrial handling processes which are best represented by the dustiness test.

## 3. THE WARREN SPRING LABORATORY ROTATING DRUM TEST

The Warren Spring Laboratory rotating drum (HSE-WSL) is comprised of a dust generator and a dust sampler. The focus of the investigation reported in this paper is the dust generation process. A detailed description of the testing procedure using the complete set up of the HSE-WSL test can be found in the technical literature (Health and Safety Laboratory, 1996). The rotating drum comprises a stainless steel drum of 0.3m diameter with conical ends. The length of the cylindrical drum body is 0.228m and the length of each conical end section is 0.13 m. Eight vanes are eccentrically mounted on the inside of the cylindrical body of the drum, to promote the lifting and falling action on the material. The drum rotates on a pair of rollers mounted on a support frame. The rotation of the rollers and hence drum are driven by a variable speed motor, set at 30 rpm. A schematic representation of the tumbling mill may be seen in Fig. 2.

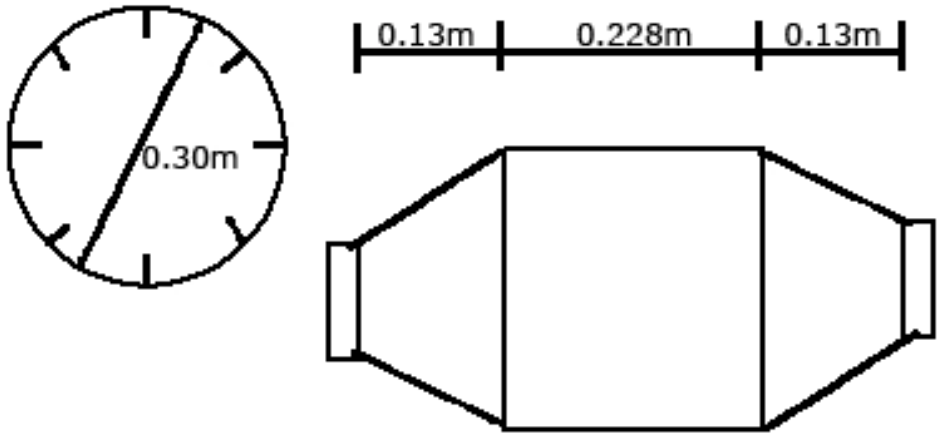


Fig. 2 - The HSE-WSL rotating drum. The cross section of the drum also presents the blades attached in the inlet of the drum

## 4. MATHEMATICAL MODELLING OF BREAKAGE PROCESS OF TUMBLING MILL

The breakage of the particle charge within the rotating tumbling mill was modelled using a population balance approach, to explore if the breakage mechanisms that occur within the drum may be predicted and follow some common principles. The model was based on the concepts of the specific rate of breakage and the breakage distribution function. The background to the adoption of this approach is outlined in detail by Austin et al., (1994). The specific rate of breakage $S_j$, is the probability of a particle from size fraction j being broken in unit time (specific tumbling time interval) (Rhodes, 2003). The breakage distribution function b(i,j) gives the probability that a particle of size fraction j breaks into a particle of size fraction i where $j < i$ (a lower number size class refers to a size fraction of greater dimension). The modelling of the tumbling mill breakage process is based on the hypothesis that the disappearance rate of particles in a given size interval can be proportional to the amount of that size remaining. The population balance equation is given as Eq. 1. (Austin et al., 1984).

$$\frac{dw}{dt} = -S_i w_i(t) + \sum_{j=1}^{i-1} b_{i,j} S_j w_j \quad (i \geq j+1) \tag{1}$$

Where $w_i$ is the mass fraction of all particles in the tumbling drum that fall into size class $i$, $S_i$ the breakage rate of particles in size class $i$, and $b_{i,j}$ is the breakage function , which refers to the breaking of the size interval $j$ relative to the size class $i$. If only the top size fraction is considered then Eq. 1 can be rewritten to a more simplified format shown in the following Eq. 2.

$$\frac{dw_i}{dt} = -S_i w_i \tag{2}$$

The integration of Eq. 2 gives following Eq. 3:

$$\ln \frac{w_i(t)}{w_i(0)} = S_i t \tag{3}$$

Where $w_i(0)$ is the relative amount of material of size $i$ in the mill at initial time (zero).

### 4.1 Assistance of the Breakage Modelling Process by Experimentation

In order to model the breakage process of the tumbling mill and to calculate the specific rate of breakage ($S_i$) and the breakage distribution function b(i,j) some data were generated from experiments. Modelling on the tumbling mill generated for four single size limestone fractions. Hence, the limestone was separate by sieving into four distinct size fractions of 150g, which were namely 3.35 to 2.36mm, 2.36 to 1.7 mm, 1.7 to 1.18mm and 1.18 to 0.85mm. The single fractions were tested at various tumbling time intervals as shown in Table 1.

Table 1- Single fractions of limestone and tumbling time intervals used to investigate the dynamics of the WSL tumbling mill.

| Limestone Fractions | Tumbling Time (minutes) |
|---|---|
| 3.35x2.36mm<br>2.36x1.7mm<br>1.7x1.18mm<br>1.18x0.85mm | 1 2 3 4 5 7 9 15 |

At the end of each experiment the limestone particles and fine material were recovered from the mill and sieved using a $\sqrt{2}$ sequence of sieves from the top size of the feed down to 53μm.

### 4.2 Analysis of Test Results

For each of the four size fractions the breakage selection function $S_i$ was calculated by plotting the natural logarithm of the relative amount of material greater than a size $i$

against the cumulative tumbling time. Fig. 3 presents the particle size distribution of the -3.35+2.36mm fraction as produced after different tumbling times. Fig. 4 shows a plot of the mass retained against the cumulative tumbling time. Fig. 5 presents the approximation of the data to first-order kinetics and the specific rate of breakage values ($S_i$) obtained for the different single size fractions.

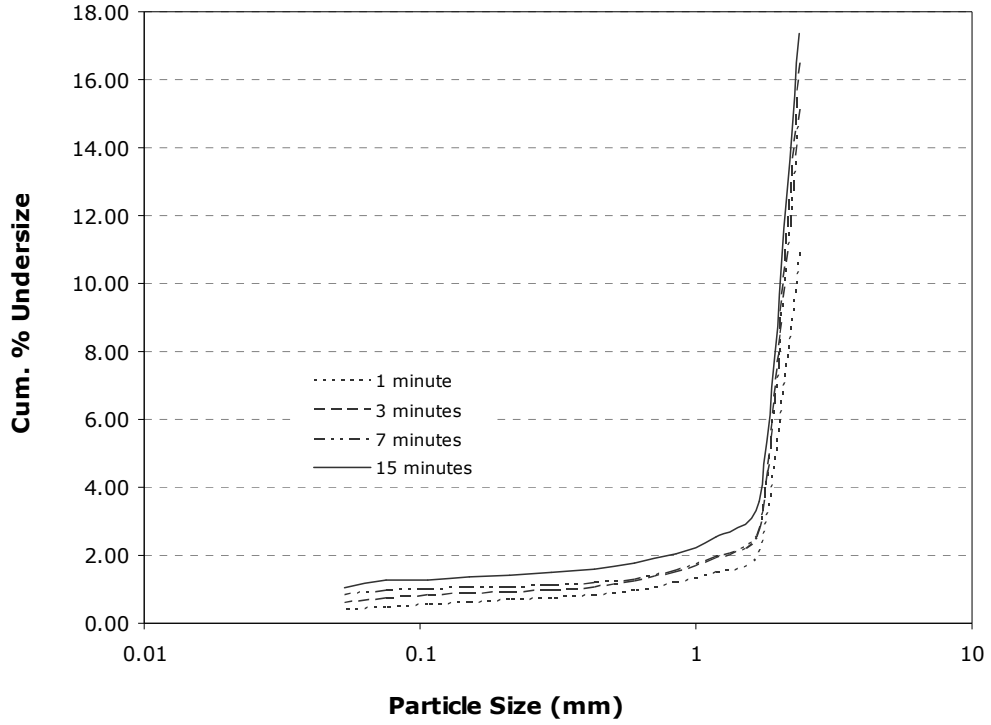


Fig. 3 - The particle size distribution of the -3.35+2.36mm fraction produced for tumbling times 1, 3, 7 and 15 minutes

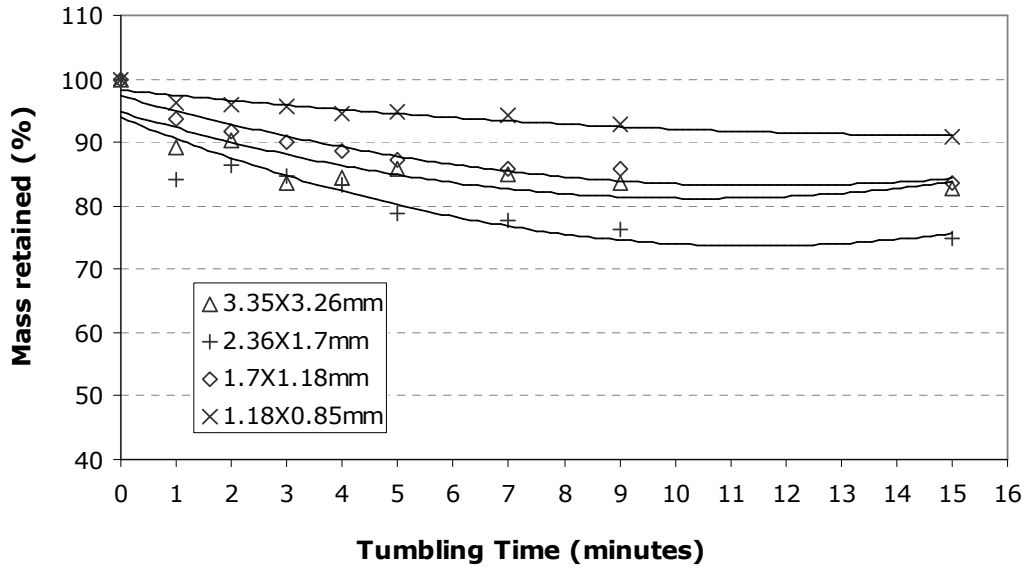


Fig. 4 - Percentage of mass retained against tumbling time for all tested fractions

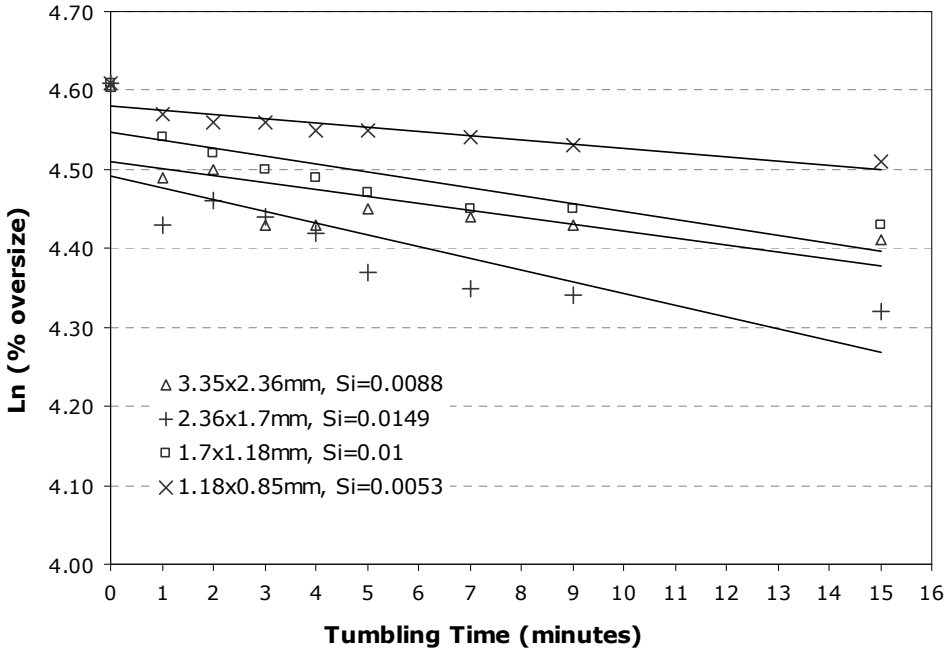


Fig. 5 - Natural logarithm of the percentage oversize plotted against the sample charge tumbling time

An analysis of the resultant particle size distribution indicated that greater the tumbling time, the finer were the resultant particle size distributions. The effect that increased tumbling time had on the particles tested was particularly intensive at smaller sizes (i.e. below 1.7mm for the -3.35+2.36mm fraction). Hence increasing the tumbling time causes an increase in the concentration of fines, implying that mainly surface breakage occurs due to the wear of particles on its surface by abrasion and chipping.

The values obtained for the specific rate of breakage parameters for the -2.36+1.7 mm and 1.7+1.18 mm fraction, were higher than the coarser fraction -3.35+2.36mm. It was concluded that these two fractions have a greater potential to break, thus limestone exhibits selective breakage. The -1.18+0.85 mm presents the lower specific breakage rate. A similar trend has been observed when the percentage of mass retained was plotted against the tumbling time. Fig. 4 shows that the disappearance rates are more rapid initially for tumbling time up to 4 minutes, whilst for increasing times, past 4 minutes, the rate of breakage is lower. For tumbling times greater than 9 minutes no further breakage was observed. This observation supports the proposition that as the surface asperities are removed, the particles become smoother and the rate of production of fine progeny will decrease.

Previous studies (Petavratzi et al., 2007) were conducted to explore the effect that tumbling time (1 to 5 minutes) has on dust yield (for a limestone sample of 100g, <3.35mm). They found a linear relationship between the tumbling time and dust yield. The dust yield increased rapidly for tumbling times up to 3 minutes. Also dustiness tests on a single size limestone fraction (10mm particles) showed that increasing the tumbling time from 1 minute to 3 minutes doubled the dust yield. This result comes in

good agreement with the disappearance rates observed for the single size fractions of limestone, which also increase with extended tumbling time up to 4 minutes.

The values of the breakage distribution function b(i,j) were used to describe the size distribution of the breakage product. Some of these results are presented in Table 2. In addition the specific rate of breakage and the breakage distribution function were used to predict the product size distribution of a limestone feed <3mm (150g). The product size distribution was also determined by sieving and the results were compared with the predicted ones. Both the feed and measured product size distributions are expressed as fractions of the mass retained at a particular particle size interval to the total mass of the sample. The product size distribution was predicted using the following Eq. 4 (which results from the modification of Eq. 1). Since wi=yiM and wj=yjM, where M is the total mass of feed material and yi is the mass fraction in size interval i, then we can write a similar expression for the rate of change of mass fraction of material in size interval, i with time (Eq. 4) (Rhodes, 2003). Some of the results obtained are presented in table 3.

$$\frac{dy_i}{dt} = \sum_{j=1}^{j=i-1} \left\{ b(i,j) S_j y_j \right\} - S_i y_i \qquad (4)$$

Table 2 - The specific rate of breakage and breakage function for the tumbling mill and tumbling time 3 minutes

| Interval (mm) | 3.35x2.36 | 2.36x1.7 | 1.7x1.18 | 1.18x0.85 |
|---|---|---|---|---|
| Sj | 0.0088 | 0.0149 | 0.01 | 0.0053 |
| b(1,j) | 0 | 0 | 0 | 0 |
| b(2,j) | 0.83 | 0 | 0 | 0 |
| b(3,j) | 0.05 | 0.84 | 0 | 0 |
| b(4,j) | 0.02 | 0.05 | 0.71 | 0 |

An analysis of the data presented in Table 3, concludes that the predicted and measured product size distributions present were in good agreement. A similar conclusion was drawn for the results obtained for the other tumbling times employed. Thus, with a set of specific rate of breakage and breakage function values for a given feed material, the product size distribution after a given time in the WSL mill may be determined.

Table 3 - Prediction of the product size distribution of a limestone <3mm feed, for 150g, tumbling time 3 minutes. The product size distribution is also determined by sieving (measured product)

| Interval (mm) | 3.35x2.36 | 2.36x1.7 | 1.7x1.18 | 1.18x0.85 |
|---|---|---|---|---|
| Interval No j | 1 | 2 | 3 | 4 |
| Feed Fraction | 0.21 | 0.18 | 0.15 | 0.1 |
| Prediction for product Fraction | 0.19 | 0.17 | 0.15 | 0.1 |
| Measured product Fraction | 0.25 | 0.19 | 0.13 | 0.09 |

The results of the population balance modelling of the breakage process indicate that the breakage process can be satisfactorily predicted using first-order kinetics. This implies that the breakage mechanisms in the mill are predictable and consequently the WSL drum test can be considered to simulate common handling processes. Therefore it can be concluded that tests such as the ones described in this paragraph, could prove good predictors of the material behaviour under certain processes and its dependency to dustiness levels. These observations also suggest that optimisation of certain industrial processes to lower dust emissions would be possible and could be predicted from the laboratory tumble mill test.

## 5. FURTHER EXPERIMENTAL STUDIES ON WSL ROTATING DRUM

Although some interesting preliminary conclusions were drawn from the experiments performed to study the kinetics of the HSE-WSL tumbling drum, it was not possible to distinguish what was the impact of each one of the mechanisms (impact, abrasion) that acted on the particles in the mill. Consequently, a further experimental and computational study was conducted in an attempt to identify the mechanisms of dust production in the tumble mill. A series of laboratory experiments were conducted using a high speed video camera, to record the tumbling action of the particles within the mill. The computational modelling was undertaken using the three dimensional discrete element modelling method (DEM) The computational models were constructed using the commercial PFC$^{3D}$ (Itasca, 2003) code and are presented in a later section.

### 5.1 Video Recording of Tumbling Action of Particles

The tumbling motion of the particles in the WSL drum was recorded using the Kodak EM high speed video system. The Kodak EM (electronic memory) system records high speed events and provides immediate slow-motion playback. The system consists of a Kodak ektapro hi-spec processor, a Kodak ektapro hi-spec imager, a monitor, light sources and a PC. The experimental set up can be seen in Fig. 6.

To permit an interior view of the rotation of the particles, Perspex observation windows were fitted to the conical ends of the drum. The video images were recorded perpendicularly through one of the Perspex observation windows. In addition, a pair of spot lights was set at each conical end to improve the detail of the images. The video system recorded directly on solid state memory for 20 seconds at 1000 frames per second. The full picture size definition was 240 pixels horizontal, 200 pixels vertical and with 625 pixels grey levels. Images were downloaded through a Kodak interface to a 300 MHz Pentium II personal computer for subsequent post processing.

For these studies, limestone particles of 10mm single size were used at charge masses of 150g, 200g and 400g. The rotation speed of the mill was kept constant at 30 rpm. The tumbling action was recorded until the memory of the video system was full. An edited fraction of the resultant video frames (up to 500) were downloaded to a personal computer for further processing.

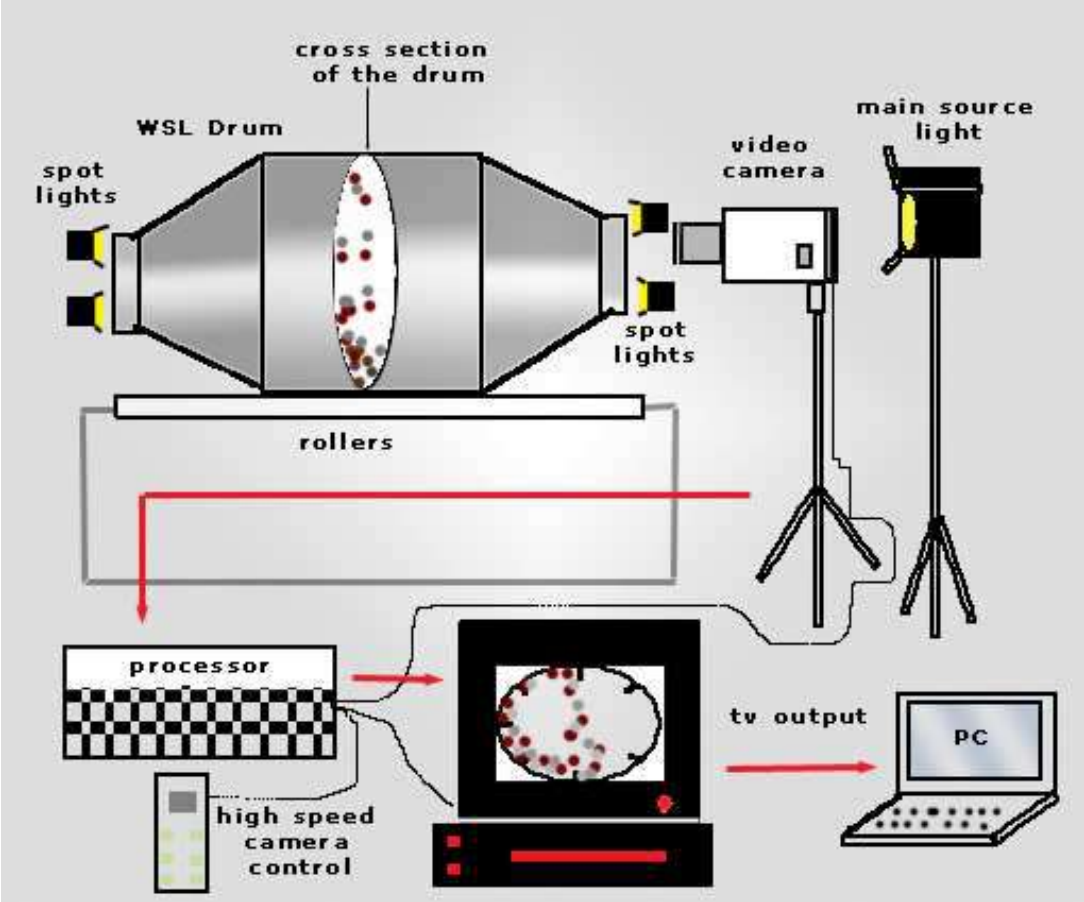


Fig. 6 - The experimental setup of the recording of the tumbling drum

### 5.2 Experimental Observations using High Speed Video System

An analysis of the recorded video images of the tumbling process showed that the limestone particles were transferred with the help of the lifter bars to the top of the drum, from where they were allowed to follow a free fall trajectory and eventually impact at the bottom of the drum. The same process continued several times until the test was completed.

The size of the limestone particles was smaller than the lifter bars (25mm), therefore the particles remained in contact with the sides of the drum and the inner edge of the blades until the influence of gravity was greater than any other applied force, normally at a position close to vertical. For sample charge masses of below 400g this behaviour resulted in the impact of particles in discrete events and not continuously as a cluster of particles sliding off the lifter bars. During the impacts it was also observed that the particles did not fragment, implying that dust was not generated due to volume breakage of particles. Also, particle to particle impacts and interaction was low for small masses of limestone (i.e. for mass charges of 150g and 200g). For samples of mass greater than 200g, particle to particle interactions were present due to sliding of particles caused by the rotation of the mill as well as due to impact between particles during free fall. For

sample masses greater than 200g impact between particles during freefall were observed at higher rates.

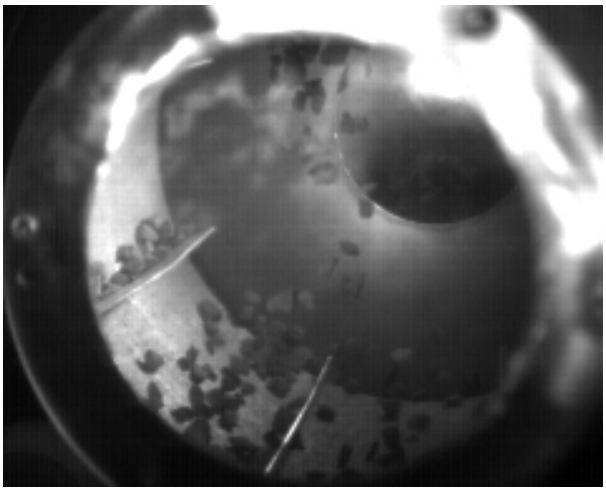

Fig. 7 - A video still of the recorded tumbling action of the 10 mm limestone particles in the HSE-WSL mill recorded by the high speed video system

From an analysis of the video stills it was concluded that during their capture and rotational transport the particles would diminish their size due to abrasion during frictional sliding and inter particle contacts. This abrasive action would cause surface asperities on the particle to be removed and generate fine dust fractions.

It can be considered that for breakage of a particle to occur and new fracture surfaces to form then the particle must possess sufficient kinetic energy. The kinetic energy of the particles in the mill is therefore closely related to the probability for breakage to occur. If breakage does not take place, then the particles do not generate sufficient kinetic energy. The kinetic energy of the particles was determined by tracking the trajectories of individual particles on a frame by frame basis from the top of the mill to the impact point. The velocity ($v$ in m/sec) of the particles was calculated from the change in horizontal ($dx$) and vertical ($dy$) distances as a function of time ($dt$) using Eq. 5.

$$v = \sqrt{\left(\frac{dx}{dt}\right)^2 + \left(\frac{dy}{dt}\right)^2} \quad , [m/s] \tag{5}$$

The kinetic energy of the particles is given by equation 6, where $m$ is the mass of test sample (i.e 150g or 200g) and $v$ (m/sec) is the velocity of the particles.

$$E_k = \frac{1}{2} m v^2 \quad , [J] \tag{6}$$

The particles (150g, 10mm) and reached their maximum velocity, thus their uppermost kinetic energy, close to impaction. The particle velocity was 1.59 m/sec, whilst the

kinetic energy was determined as 0.001 Joules. The velocity and kinetic energy results represent average values from repetitive tests. The experimental results for the kinetic energy of the limestone particles are compared with modelling data, whereas the minimum kinetic energy requirements for fragmentation to occur are calculated and presented in the following paragraphs.

### 5.3 Energy Losses upon Impact

Upon the impact of the falling particles with the bottom of the drum the vast majority of the kinetic energy is lost and therefore not available to form new surface on breakage. However, any small asperities in the line of these collisions will experience extreme stress and be destroyed and produce fine progeny. The amount of energy loss upon impact can be estimated by the Coefficient of Restitution (CoR) of the particle-steel impact. The CoR was calculated using a simple test where a limestone particle was released from a measured height equal to the diameter of the mill. The Kodak EM system was used to record the impaction of the particle onto steel surface, whilst the trajectory of the particle was tracked down frame by frame so as to get an accurate measurement of the rebound height. The experiment was repeated three times and an average rebound height determined. The coefficient of restitution was then calculated as being the square root of the ratio between the average height of rebound and the drop height. The determined value of CoR was 0.31. The coefficient of restitution can also be defined as the ratio between the velocity before and after impact. Assuming a particle velocity prior to impact equal to 1 m/sec it can be estimated that for a coefficient of restitution of 0.31 approximately 90% of the kinetic energy would be lost on impact. It was observed, similarly in the tumbling drum test, that fragmentation did not occur. The energy losses were therefore attributed to kinetic energy dissipation (i.e. particles spin) or transformation of the kinetic energy to other energy forms (i.e. heat, sound) and lost to transmission through the base of the sample. Therefore, only a small proportion of the kinetic energy during impact was absorbed by the particle, which was not enough to break it.

An analysis of the experimental data obtained from the high speed video system test showed further that the HSE-WSL test simulates well the industrial processes, where dust is generated due to abrasion of the rock particles such as on conveyor belts, sieves, haulage roads etc.

Fig. 8 - The limestone particle at the highest position after rebounding on the steel surface.

## 6. COMPUTATIONAL MODELLING OF TUMBLE MILL

Computational modelling of the tumble mill was undertaken to provide a more fundamental understanding of the mechanisms of dust generation that were observed within the mill and also to identify the mill parameters that affect the quantity of dust produced. The modelling was undertaken using the distinct element modelling code PFC$^{3D}$ Version 3.0 produced by Itasca (Itasca, 2003). Although the DEM method was developed in 1979 (Cundall and Strack, 1979) it was only around 1990 that Mishra and Rajamani (1992) adapted the scheme to solving tumbling mill problems as this method was too demanding for the computational technology at that time. The distinct element method has now been adopted as an established method for predicting particle motion and energy distributions in tumbling ball mills (Djordjevic, 2003 & 2004; Morrison and Cleary, 2004; Li, 2002; Mishra and Chenug, 1999). More recently application of the DEM technique for modelling power draw demonstrated that the numerical approach produced results that were close to monitored values and comparable with the results obtained using empirical based models (Djordjevic, 2003; Cleary, 2001).

### 6.1 Discrete Element Numerical Modelling

The DEM models may be used to simulate the movement and interaction of spherical elastic particles during discrete intervals of time using a time stepping explicit numerical scheme (Cundall and Strack, 1979). The particles interact with adjacent particles and boundaries known as walls when contact is detected. These mechanical interactions are governed by Newton's dynamic laws of motion and contact logic. The DEM method uses a soft contact logic, whereby the particles are allowed to overlap, to predict the forces and moments generated due to particle to particle and particle to wall interactions. These forces and moments are then used to calculate the displacements and rotations of the particles by numerical integration of Newton's dynamic law of motion. Non-spherical particles may be constructed using a clump logic that allows individual particles to be permanently joined together to represent a non-regular particle

agglomeration. As the system behaves in an elastic manner, energy losses in the system has to be accounted for explicitly using a damping formulation that modifies the particle velocities and forces. The numerical method used to integrate the dynamic law of motion is the centred finite difference method whereby the forces and displacements of each individual particle is determined at individual time step with velocities being kept constant during the time step. This numerical method requires that the time step is of a size whereby non-linear responses of the system such as non-linear changes in magnitudes and directions of velocity do not occur during each calculation step.

### 6.2 Modelling Methodology

The DEM method adopts a soft contact logic where overlaps of the contacting particles are allowed and used to determine the contact forces. PFC$^{3D}$ has two inbuilt contact laws; firstly a linear law where the contact normal and shear force acting are linearly related to the degree of normal overlap and shear displacement, and secondly a more complex Hertzian non-linear contact law whereby the normal stiffness of the particle increases with increasing overlap to account for the greater contact surface when two spherical particles are pressed together. A study whereby both contact laws have been utilised for the modelling of tumble mills is described by Mishra (2003). For the purposes of the modelling the linear law was adopted and the key features are summarised below.
For the linear law the normal contact force is given by the following Eq. 6.

$$F_i = K^n.U^n.n_i \quad , [N] \tag{6}$$

Where
$F_i$ = force acting normal to the surface at the point of contact [N],
$K^n$ = stiffness of the particle [N/m],
$U^n$ = magnitude of overlap [m], and
$n_i$ = normal unit vector to the contact plane.

The shear force acting at the point of contact is calculated incrementally by adding an incremental force determined using the following Eq. 7 at each time step.

$$\Delta F_i^s = -K^s.\Delta Ui^s \quad , [N] \tag{7}$$

where
$\Delta F_i^s$ = increment of shear force [N],
$K^s$ = shear stiffness of particle [N/m], and
$\Delta Ui^s$ = increment of relative shear displacement (corrected for rotation) [m].

Thus at the end of every time step, the shear force, $F_i^s$, is updated by adding $\Delta F_i^s$ to the existing value of $F_i^s$ after it has been corrected for rotational movement of the contacting plane during the time increment. The normal and shear force vectors can be added to form one contact force vector $F_i$ as follows.

$$F_i = F_i^n + F_i^s \quad , [N] \tag{8}$$

*6.2.1 Limiting frictional force*

The magnitude of the shear force is limited by the maximum resistance to frictional sliding. In PFC3D frictional sliding is controlled by a Coulombic law Eq. 9.

$$F_{s(max)}=\mu.F_n \quad , [N] \tag{9}$$

where
$F_{s(max)}$ = maximum allowable shear force [N],
$\mu$ = friction coefficient, and
$F_n$ = normal force [N].

This new force vector is then used to determine the resultant force and moments acting on the two contacting particles.

Frictional sliding is a process whereby energy loss is directly modelled in the system. It has been shown by Mishra and Rajamani (1992), Mishra and Thornton (2001) and Van Nierop et al. (2001) that the power draw of mills depends on the coefficient of friction and is particularly sensitive to this parameter at higher mill speeds. Also the process of dust generation observed in the tumble mill i.e. particle to particle and particle to steel attrition occurs as a result of frictional sliding.

*6.2.2 Damping logic*

Removal of excess energy from the particulate system occurs during frictional sliding of the particles. However energy loss due to frictional sliding is not usually sufficient to simulate all the energy losses within the system, for instance localised plastic deformation at the point of contact, particle heating, attenuation of energy within the walls of the mill and sound energy losses, and therefore the motions of the particles will then not be sufficiently damped. A damping of the dynamic force-displacement law is thus required to accurately simulate the forces and motions of the system. PFC$^{3D}$ has several in-built damping laws. The damping logic can either be local non-viscous whereby the velocities of the particles are reduced by a factor, to dampen down motion, or viscous damping whereby numerical equivalents to normal and shear dashpots are added at each contact. Non-viscous damping is not appropriate for particles in free flight and therefore viscous damping was utilised within the modelling. In viscous damping a damping force is added to the contact force. The damping force is dependant on the particles impact velocity and is determined using following Eq. 10.

$$D_i = C_{i.}[V_i] \quad , [N] \tag{10}$$

where
$D_i$ = damping force [N],
$C_i$ = damping constant [kg/s], and
$[V_i]$ = magnitude of the particle velocity [m/s].

The damping constant used in Eq. 10 is determined by using Eq. 9.

$$C_i = \beta_i.C_i^{crit} \quad , [kg/s] \tag{11}$$

where
$C_i^{crit}$ = critical damping constant [kg/s] and
$\beta_i$ = critical damping ratio.

The critical damping constant depends on the mass and stiffness of the particle and is given by following Eq. 12.

$$C^{crit} = 2.(m.k_i)^{0.5} \quad , [kg/s] \tag{12}$$

The critical damping ratio is required as an input parameter when using the viscous damping models and can be determined by calibration with the measured coefficient of restitution of the particles. If the critical damping ratio is <1 then the response is of decaying oscillations and the particle is said to be under damped. This is the natural condition when the coefficient of restitution is greater than zero.

### 6.3 Numerical Modelling of Tumble Mill

The tumble mill simulation can be considered to comprise of two components which were namely the mill itself and the mass of particles inside the mill.

#### *6.3.1 DEM model of the particles*

The sub-angular equate shaped particle used in the laboratory experiments was represented as a bonded agglomerate of six spherical elastic particles. The unbreakable agglomeration was formed using clump logic. This was undertaken to ensure that upon impact the centre of gravity of the particle did not lie directly over the point of impact and thus the particle may spin on impact replicating the behaviour that is observed in the tumble mill. A picture of a typical particle is shown in Figure 9.

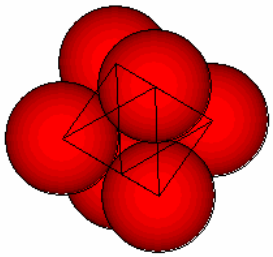

Fig. 9 - PFC$^{3D}$ particle formed by clump logic

#### *6.3.2 Material Properties*

The friction angle of the wall/particle contact was obtained by undertaking a simple tilt test whereby a single particle was placed on a flat sheet of stainless steel which was tilted until the particle started to slide. The angle of sliding was measured to provide an estimate of the friction angle. This simple experiment was repeated several times and the average friction angle determined using this method was 21$^o$. To ensure that the

friction angle produced the correct trajectory of the particle in the mill, the trajectory of a single particle around the drum was compared to that derived from the video of the tumble mill. It was considered that if the particle traced a similar trajectory to a particle in the actual mill the frictional parameters for the walls and particles would be correct.

As previously discussed the coefficient of restitution of the particles was determined by experiment to be 0.31. In the construction of the model viscous damping was adopted, which required the determination of the critical damping ratio. The coefficient of restitution and critical damping ratio can be related. In the model the relationship was determined by calibration by simulating the dropping of a single particle onto a steel plate and measuring its rebound height. The importance of this parameter was also highlighted by Djordjevic (2005), who found from parametric studies that the viscous damping ratio of the particles is a very significant parameter in the DEM of tumble mills.

The normal and shear stiffness (Table 4) were selected from those previously used for the modelling of particles in a tumble mill (Djordjevic, 2005). The values are lower than those typically measured for real rock particles. However, Djordjevic found that the predicted power draw remained constant within a narrow range on varying the stiffness over the range of 10 to 5,000 $kNm^{-1}$. He concluded that the results of the simulation are not particularly sensitive to the stiffness parameter and that it is desirable to reduce the particle stiffness to a value below the measured values to ensure that the simulation can be undertaken in a reasonable amount of time.

Table 4 - Detailed physical properties of the particles used within the DEM simulation models

| Density $kg/m^3$ | Coefficient of friction | Coefficient of Restitution | Particle stiffness N/m | |
|---|---|---|---|---|
| | | | Normal stiffness | Shear stiffness |
| 2800 | 0.5095 | 0.31 | $4 \times 10^5$ | $3 \times 10^5$ |

*6.3.3 Model of tumble mill*

The model of the tumbling mill consisted of a complex polygonal assembly of rectangular walls. The walls act as boundary conditions on the particle assembly. If contact is detected between a particle and a wall then a contact logic is used to determine the nature if the interaction. The parameters that define the wall and govern its interactions with contacting balls are the normal stiffness, shear stiffness and frictional coefficient. The physical system consists of a series of walls representing the mill (Figs. 11 and 12). The stiffness and frictional parameters of the walls were assumed to be equivalent to the parameters of the particles and are given in Table 5.

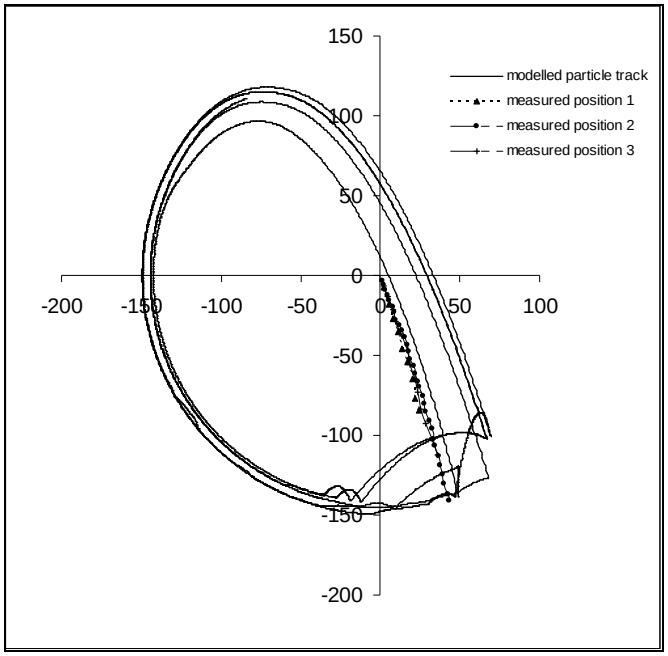


Fig. 10 - Comparison between trajectory measured in the laboratory experiment and that predicted by the DEM model

Table 5 - Stiffness and frictional parameters of the drum walls

| Stiffness N/m | | Friction coefficient |
|---|---|---|
| $k_n$ | $k_s$ | $\mu$ |
| $4 \times 10^5$ | $3 \times 10^5$ | 0.5095 |

### 6.4 Numerical Modelling Programme

The computational model simulations of the mill can be divided into two sets. The first set was undertaken to investigate the affect of particle mass on the generation of dust within the tumble mill, whilst the second set was undertaken to asses the affect of rate of rotation of the mill on the characteristics of dust generation in the mill whilst keeping the particle mass constant.

Four model simulations of the laboratory experiments were undertaken but with different particle masses. The four simulations are summarised in Table 6 below and represent particle masses of 150 grams, 200 grams, 300 grams and 400 grams.

Table 6 - Number of particles simulated for each mass fraction in PFC model

| | Total mass (grams) | Number of particles |
|---|---|---|
| Model 1 | 150 | 180 |
| Model 2 | 200 | 264 |
| Model 3 | 300 | 396 |
| Model 4 | 400 | 528 |

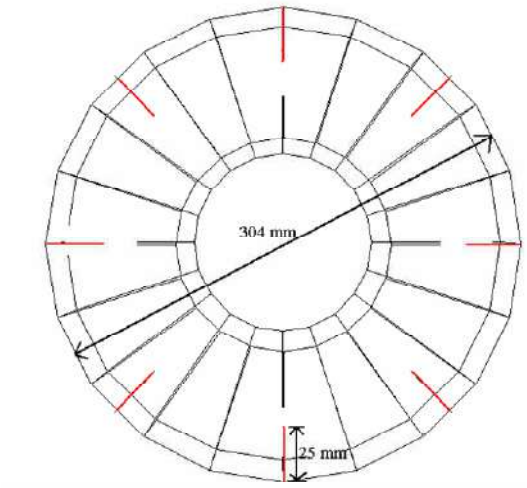


Fig. 11 - End elevation view of the WSL drum

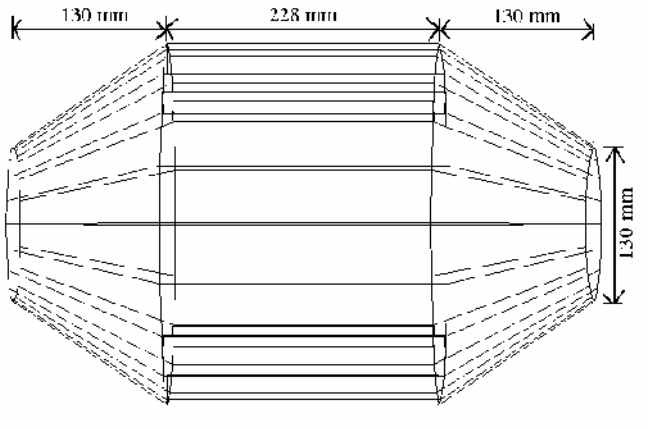


Fig. 12 - Side elevation view of the WSL drum

The speed of revolution of the mill for this set of simulations was 30 revolutions per minute, equivalent to that used in the laboratory tests. The critical velocity of the computer simulation of mill was determined to be 66 revolutions per minute, thus the modelled speed represented approximately 48% of the critical speed. The adopted method involved firstly the generation of the clumped particles in the centre of the mill. The particles were then allowed to settle under gravity at the base of the drum prior to the commencement of the revolutions. The stable time step was $6.58 \times 10^{-6}$ sec and each model was run for 3,000,000 steps representing 19.74 seconds of rotation. During the simulation, historical data files logged the frictional energy, kinetic energy and the boundary energy at 1000 step (0.00658 second) intervals.

*6.4.1 Effect of sample size on energy used for attrition processes*

Figure 13 illustrates the prediction of the amount of energy dissipated due to frictional sliding, that is the identified mechanism of dust generation. Again the energy rate due to

frictional sliding increased approximately linearly with mass of particles in the mill at the rate of 0.0009 joules/sec/gram. The increase of the energy absorption rate due to frictional sliding with increasing mass predicts that production of fines should increase with mass of material within the mill. The increase in the volume of fines produced would be expected to generate a greater volume of dust produced. This conclusion has been justified by earlier experiments on the dependency of the mass of material to the dust yield, for a limestone sample. These investigations have shown that dust levels increase as the sample mass increases up to 400g. Also in a different instance a positive correlation between fines accumulation in the mill and dustiness levels has been observed. Dustiness measurements are normally influenced by several parameters such as material properties (e.g. particle size, moisture content) and operational parameters (e.g. tumbling time). Therefore it is with caution that the modelling prediction of increasing frictional energy with mass should be used to infer the increased dust production in the tumble mill.

The percentage of energy draw from the tumble mill that was used in frictional sliding is shown in Figure 14. The modelling indicates that with increasing mass the amount of energy that is utilised for frictional sliding increases from 23.5 % of power draw for 150 grams particle mass to 30 % for 400 grams mass.

An analysis of the results presented on Fig. 14 may conclude that a greater degree of the power draw from the mill is used to produce abrasion and therefore dust. This was attributed to the greater degree of particle to particle collisions that occur with a higher mass of material and hence a greater number of particles in the mill. The modelling also indicates that once the mill reaches a steady state then the total amount of energy used in frictional sliding will be directly proportional to the tumble time i.e. it would be expected that the dust generated would increase as a linear function of time. This was also inferred in dustiness testing where it was found that an increase in testing time corresponds to a linear increase in the volume of dust generated.

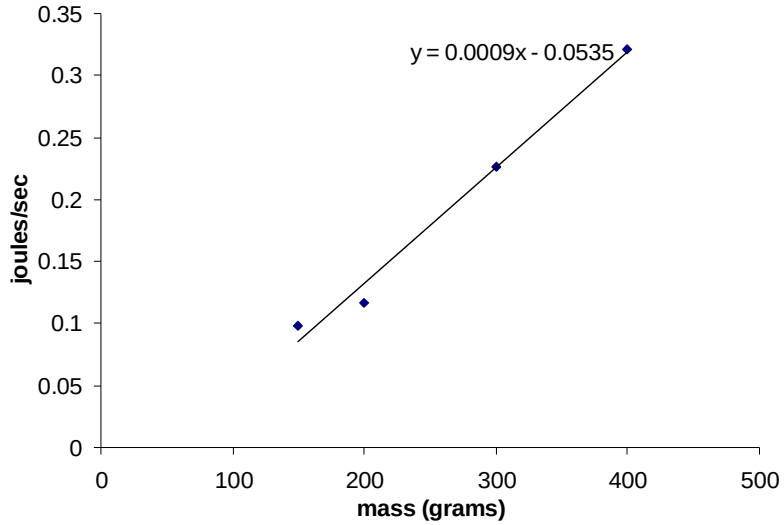


Fig. 1310 - Rate of energy dissipation due to frictional sliding as a function of total mass in PFC model

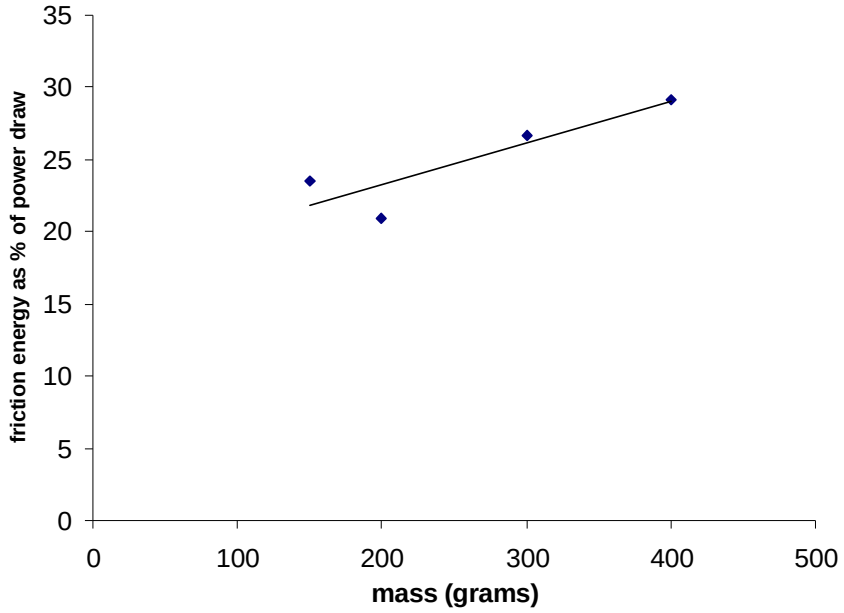


Fig. 14 - Friction energy rate as percentage of power draw against mass of sample in PFC model

*6.4.2 Affect of mill rotational velocity on dust generation and power draw*

A further set of model simulations were performed for a particle mass of 200 grams, whereby the affect of the rotational velocity of the mill on power draw and dust production was investigated. The general methodology adopted was the same as for the first set of models, with each simulation representing 19.75 seconds of rotation. However the rotational velocity of the drum was varied to simulate critical velocities of 20 %, 35%, 48 %, 65%, 73 %, 90% and 99%. The trajectories of a single particle for each of these velocities are shown in Fig. 15.

The affect of the mill rotational velocity was investigated in terms of net power draw, frictional energy dissipation and the ratio between frictional energy rate and power draw. Figure 15 shows the affect of rotation speed on power draw and indicates that the maximum power draw occurred at approximately 63% critical velocity.

The general shape of the graph is similar to the results of a modelling exercise by Misra and Cheung (1999) but differs in that they found that the highest mill power is drawn for mill speeds between 70 to 85% critical velocity.

The rate of energy loss due to frictional sliding at the various mill velocities is shown in Figure 16. Although there is a degree of scatter in the data the graph shows a general trend of increasing rate of energy loss due to frictional sliding with mill speed.

The frictional energy loss as a percentage of the power drawn from the mill is shown in Fig. 17. This figure clearly indicates that the minimum occurs at approximately 63% of the critical velocity of mill.

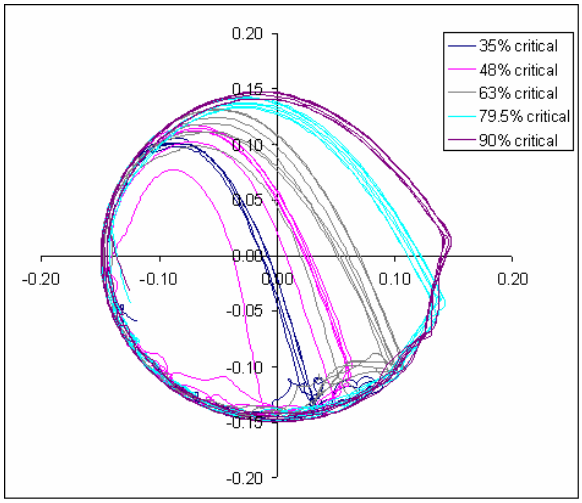


Fig. 15 - A plot of the predicted single particle trajectories in PFC model

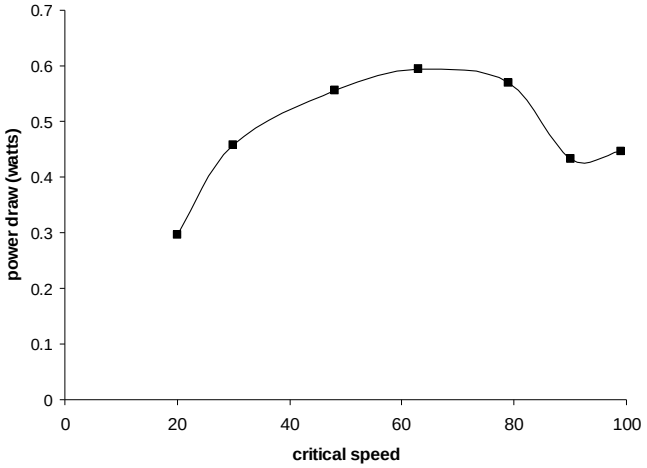


Fig. 1611 - The relationship between rotational drum speed and power draw in PFC model

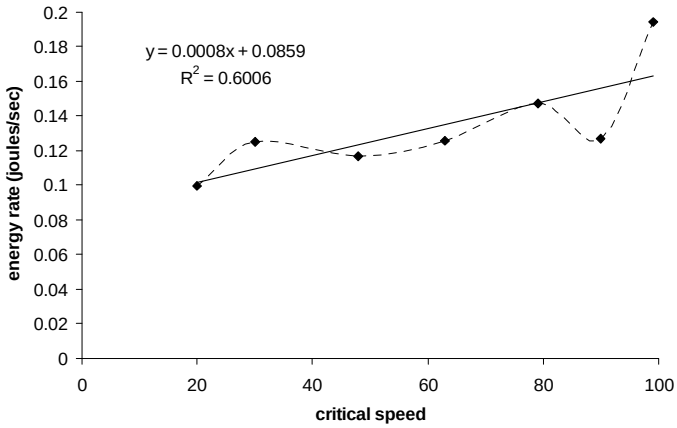


Fig. 17 - Energy loss due to friction at the various rotational speeds in PFC model

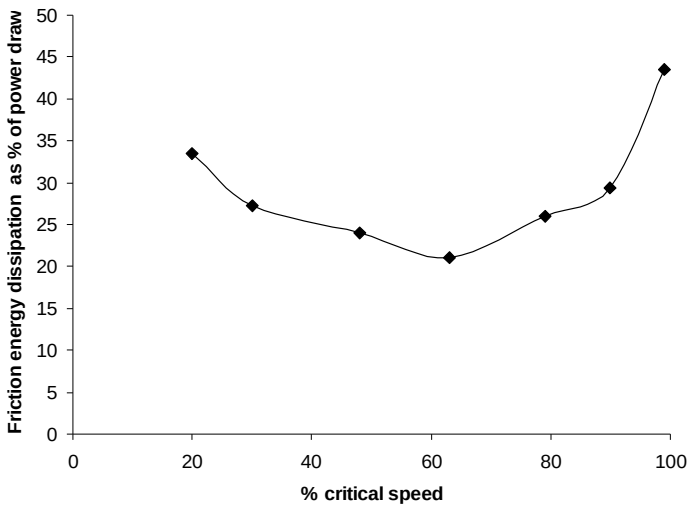


Fig. 18 - The frictional energy loss as a percentage of the power drawn for various mill speeds in PFC model

However, although the maximum power draw is predicted to occur at approximately 63% critical velocity the amount of the power draw that is used for frictional abrasion, and therefore dust generation, is at a minimum at this velocity (Figure 18). This indicates that if the drum was of a sufficient size for fragmentation to occur optimum fragmentation with minimal dust production due to abrasion would occur at approximately 63% critical mill speed.

## 7. DISCUSSION AND CONCLUSIONS

Both the experimental and computational steps have shown that dust generated in the tumbling mill is mainly due to one mechanism that of abrasion, which is caused by the frictional sliding of particles on the drum walls and over other particles.

The breakage process of tumbling mill follows the first order kinetics, which implies that the mechanisms of the tumbling mill may be predictable, whereas the HSE-WSL drum can find application on the simulation of common handling processes.

The experiments and mathematical calculations show that the particles would not have sufficient kinetic energy for fragmentation to occur for mill size used. Approximately 90% of the kinetic energy is lost on impact, leaving only a small percentage to be absorbed by the particles, which cannot break them. Two sets of PFC$^{3D}$ DEM simulation models of the mill were solved. The first set investigated the affect of mass of sample on dust production and power draw and indicated that there was a linear relationship between power draw and mass of particles in mill. The amount of energy dissipated due to frictional sliding also increased linearly with particle mass. It was conjectured that the amount of dust production would be directly related to energy used in sliding and it was therefore seen that there was a positive relationship of the dust yield produced and particle mass at a fixed rotation speed. This statement has been confirmed by earlier studies on the dependency of sample mass to the dust yield of

limestone. The second series of models investigated the effect of mill velocity on dust production. This set of models indicted that power draw was a maximum at approximately 63% critical speed but the ratio between energy loss to frictional sliding and power draw was a minimum at this speed. It was concluded that if mill was of a sufficient size for fragmentation to occur optimum fragmentation with minimal dust production due to abrasion would occur at approximately 63% critical speed.

The findings of this work indicate that the particulate matter generation potential of industrial processes that they mainly produce dust by abrasion is analogous to operational parameters of these processes. Optimisation of parameters that have the greatest influence in the process can result to dust reduction. For instance, optimising the velocity of conveyor belts or the velocity of vehicles in haulage roads could minimise the generation of particulate matter. In depth investigation of the mechanisms involved in industrial processes has proved to compare well with the dust liberation potential and it can be used to predict trends and evaluate the impact of a specific event.

**References**

Austin, L.G., Klimpel, R. and Luckie, P.T. (1984). Process Engineering of Size Reduction: Ball Milling, SME Publishers, New York.

British Occupational Hygiene Society Technology Committee (1985). Dustiness Estimation Methods for Dry Materials: Part 1, Their Uses and Standardization; Part 2, Towards a Standard Method, Science Reviews, UK, Technical Guide No 4.

Health and Safety Laboratory. (1996). Methods for the Determination of Hazardous Substances 81 (MDHS) - Dustiness of powders and materials, Health and Safety Executive, UK, MDHS 81, HMSO.

Cundall, P.A. and Strack, O.D.L. (1979). A discrete numerical model for garnular assemblies, Geotechnique, 29 (1), pp 47-65.

Cleary, P.W. (2001). Charge behaviour and power consumption in ball mills: Sensitivity to mill operating conditions, liner geometry and charge composition, International Journal of Mineral Processing, 63, pp 79-114.

Djordjevic, N. (2003). Discrete element modelling of power draw of tumbling mills, Transactions C of the Canadian Institution of Mining and Metallurgy, 112, pp C104-C114.

DJordjevic, N. (2005). Influence of charge size distribution on net power draw of tumbling mill base on DEM modelling, Minerals Engineering, 18, pp 375-378.

Higman, R.W. (1985). Dustiness testing. a useful tool, Proceedings of the 1st International Symposium on Ventilation for Contamination Control, Toronto, Ontario, Canada, pp 693-702.

Itasca Consulting Group. (2003). PFC$^{3D}$ (Particle Flow Code in 3 Dimensions) Ver 3.0, Minneapolis, USA.

Li, S. Q., Chi, Y., Li, R.T.,Yan, J.H. and Cen, K.F. (2002). Axial transport and residence time of MSW in rotary kilns: Part II Theoretical and optimal analysis, Powder Technology, 126, pp 228-240.

Lyons, C.P. and Mark, D. (1994). Development and testing of a procedure to evaluate the dustiness of powders and dusts in industrial use, Health and Safety Executive; UK, 62/1994.

Mishra, B.K. (2003). A review of computer simulation of tumbling mills by the discrete element method: Part 1 - Contact Mechanics. International Journal of Mineral Processing, 71, pp 73-93.

Mishra, B.K. and Cheung, J. (1999). Particle motion and energ distribution in tumbling mills, Powder Technology, 105, pp 222-227.

Mishra, B.K. and Thornton, C. (2001). Impact breakage of particulate agglomerates, International Journal of Mineral Processing, 61, pp 222-227.

Mishra, B.K. and Rajamani, R.K. (1992). The discrete element for simulation of ball mills, Applied Mathematical Modelling, 16, pp 598-604.

Morrison, R.D. and Cleary, P.W. (2004). Using DEM to model ore breakage within a pilot scale SAG mill, Minerals Engineering, 17, pp 1117-1124.

Napier-Munn, T.J., Morrell, S., Morrison, R.D., and Kojovic, T. (1996). Mineral Comminution Circuits. Their operation and Optimisation, Julius Kruttschnitt Mineral Research Centre, Queensland, Australia.

Petavratzi, E., Kingman, S.W. and Lowndes, I.S. (2005). Particulates from mining operations: A review of sources, effects and regulations, Minerals Engineering, 18, 12, pp 1183-1199.

Petavratzi, E., Kingman, S.W. and Lowndes, I.S. (2007). Assessment of the dustiness and the dust liberation mechanisms of limestone quarry operations, Chemical Engineering and Processing, 46, pp 1412-1423.

Rhodes, M. (2003). Particle Size Reduction: in Introduction to Particle Technology, John Wiley & Sons Ltd., England, pp 241-263.

Schneider, T. and Hjemsted, K. (1996). Documentation of a dustiness drum test, Annals of the Occupational Hygiene Society, 40, 6, pp 627-643.

Van Nierop, M.A., Glover, G., Hinde, E.L. and Moys, M.H. (2001). A discrete element method investigation of the charge motion and power draw of an experimental two dimensional mill, International Journal of Mineral Processing, 59, pp 131-148.